Surface Dependent Optical Transitions in Highly Luminescent Silicon Nanoparticles

Qi Li[1], Abhinav Parakh[2], Rongchao Jin[3], Wendy Gu[1]*

[1]Department of Mechanical Engineering, Stanford University, Stanford, CA 94305, United States.
[2]Department of Materials Science and Engineering, Stanford University, Stanford, CA 94305, United States.
[3]Department of Chemistry, Carnegie Mellon University, Pittsburgh, PA 15213, United States.

Corresponding Author: Qi Li, qilistan@stanford.edu

Abstract Surfaces can significantly alter the optical properties of nanomaterials, but are difficult to control and understand in highly reactive materials such as silicon nanoparticles. In this work, we investigate the role of the surface in controlling the optical transitions in highly luminescent silicon nanoparticles. By combining high-pressure and low-temperature experiments, we experimentally correlate the intense and narrow transitions in the UV range with the surface oxides, while the visible transition and the PL are verified to originate from the Si-ligand charge transfer band. We find that the high-pressure absorption and PL depends on the rigidity of the surface ligand . This work presents a comprehensive understanding of the optical transitions and the effect of surface ligands and surface oxidation in these highly luminescent Si NPs. The new insight into the oxidation-activated transition and pressure-dependent PL may help with engineering the band structure of other highly reactive semiconductor nanomaterials.

Full text

Since the discovery of room-temperature luminescence from porous silicon (Si) in the early 1990s, [1–3] the luminescent properties of porous silicon and colloidal silicon nanoparticles (Si NPs for short hereafter) have been extensively studied.[4–10] Due to their minimal toxicity, low cost and high abundance, silicon nanomaterials are regarded as promising candidates in applications from light-emitting diodes to bioimaging agents.[11–18] However, the optical spectra of Si NPs have been observed to be very complicated.[10] Si NPs synthesized from high-temperature gas phase deposition[19,20] or thermal annealing of hydrogen silsesquioxane[21–24] usually show structureless absorption starting from ~1000 nm (the indirect band gap) to ~360 nm (the direct T-T transition), as well as orange-to-NIR PL with a microsecond long lifetime. These results are consistent with the quantum confinement model and the intrinsic indirect bandgap of silicon (1.1 eV). On the other hand, Si NPs from solution synthesis usually show drastically different, blue PL[25–27] with a short lifetime and more intense excitonic-like absorption peaks in the deep blue to UV range.[25,26,28] These results can be ascribed to the inevitable surface contamination from chemicals and oxygen during solution synthesis and post-treatment, because surface modification[29,30] and the surface oxidation[31,32] can switch the PL from the "slow red" band to the "fast blue" band. However, the reported results from different research[32–34] are often contradictory, which is probably due to different experimental conditions.

Thus, it remains difficult to determine the structural source of optical transitions (e.g. core or surface atoms within Si NPs) and understand the detailed role of quantum confinement, surface ligands, and surface oxidation on the photoluminescence (PL) of different Si NPs. We previously reported the synthesis and optical behavior of surface-modified and heavily oxidized Si NPs with QYs up to 50-90%.[35,36] In these NPs, PL-color can be tuned by tailoring the ligand structure.[36–38] Stark spectroscopy confirmed the ligand-to-silicon charge transfer mechanism[39]. Herein, we measure the optical properties of these Si NPs at high pressure and cryogenic temperatures to understand the optical transition mechanisms. Using high pressure, we are able to modify the distance between the ligands and the Si surface, and test its effect on optical transitions. Low-temperature measurements reveal details within the PL and photoluminescence excitation (PLE) spectra that allow optical transitions to be assigned to different mechanisms. Through these studies, we confirm that the oxidation of Si surface atoms leads to intense optical transitions in

the UV range. These optical transitions differ from the band-edge transition and the PL emission of Si NPs which arise from the Si-ligand band.

Results.

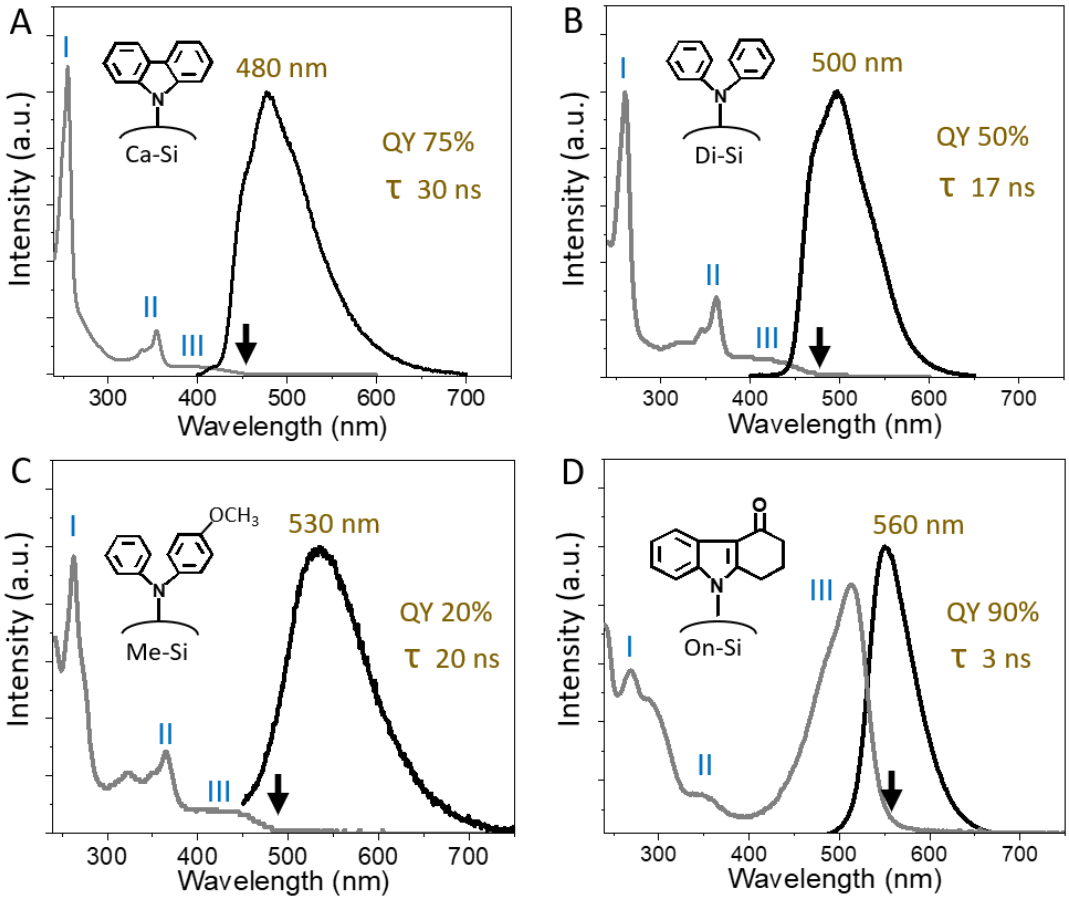

Figure 1. Absorption (gray) and PL (black) spectra of (A) Ca-, (B) Di-, (C) Me- and (D) On-Si NPs (in water). Arrows indicate the onset of absorption. Three major absorption peaks are observed: Band-I at ~260 nm; Band-II at ~360 nm; and Band-III from 400 to 550 nm.

Figure 1 displays the absorption and PL spectra of four different surface-modified Si NPs. These NPs are capped by carbazole- (abbreviated Ca-), diphenylamine- (Di-), 4-methoxyldiphenylamine- (Me-), and 1,2,3,4-tetrahydrocarbazol-4-one (On-). All of these NPs show multiple absorption transitions. The Ca-, Di-, and Me-Si NPs, show two intense and narrow absorption peaks at ~260 nm (Band-I) and ~360 nm (Band-II), as well as another broad absorption peak (Band-III) between 400 and 500 nm. The On-Si NPs show an intense peak at ~510 nm and two less intense peaks at ~360 nm and ~260 nm. The intense absorption transitions in these NPs are significantly different than other reported Si NPs. Previously reported Si NPs

generally show structureless and monotonically increasing absorption from the visible to the UV[22,40] due to the indirect band structure of silicon. In our system, the absorption onset depends on the ligands: 450 nm for Ca-Si NPs; 470 nm for Di-Si NPs; 480 nm for Me-Si NPs and 560 nm for On-Si NPs. This ligand-dependence is also observed in the PL peak wavelength: 480 nm for Ca-Si NPs; 500 nm for Di-Si NPs; 530 nm for Me-Si NPs and 560 nm for On-Si NPs.

All four Si NPs show high PL quantum yields (QY): 70 % for Ca-Si NPs; 50 % for Di-Si NPs; 20 % for Me-Si NPs and 80 % for On-Si NPs. The PL lifetimes of the four Si NPs are 30 ns for Ca-Si NPs, 17 ns for Di-Si NPs, 15 ns for Me-Si NPs and 3 ns for On-Si NPs (Figure S1). All the PL results suggest that the ligand is involved in both the HOMO-LUMO energy gap and the PL QY. Based on the measured QY and PL lifetime (τ), the rates of radiative (k_r) and non-radiative (k_{nr}) transitions in the four Si NPs can be calculated as: $\tau = 1/(k_r + k_{nr})$; $QY = k_r/(k_r + k_{nr})$. These values are reported in Table S1. Of note, the k_r of On-Si NPs (3×10^8) is one magnitude higher than the k_r of the other three samples ($\sim 10^7$). This is consistent with the intense band-III absorption (stronger transition dipole) of the On-Si NPs observed in Figure 1, which indicates that the band-III absorption and the PL may arise from the same structural origin.

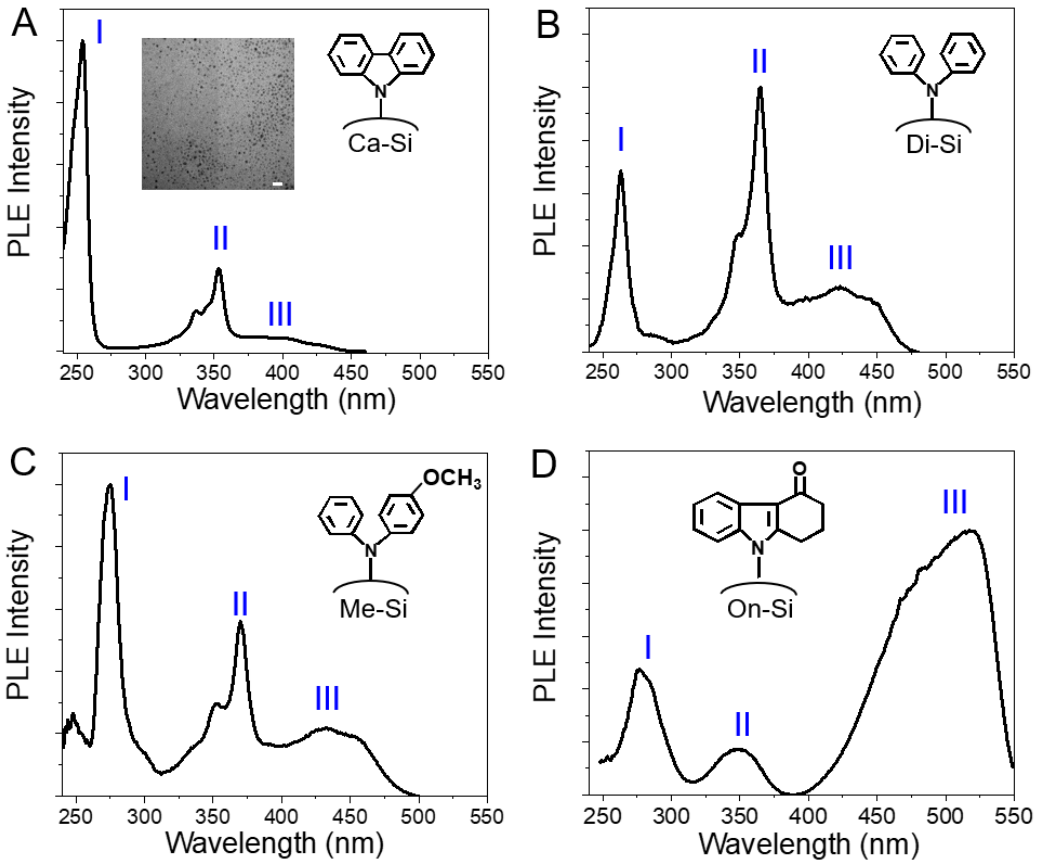

Figure 2. PL excitation spectra of (A) Ca-Si NPs, (B) Di-Si NPs, (C) Me-Si NPs and (D) On-Si NPs (in water). Three major excitation peaks are observed: peak I at ~260 nm; peak II at ~360 nm; peak III from 400 to 550 nm. Inset of (A) is a TEM image of the Si NPs, scale bar = 10 nm.

PL excitation (PLE) spectra of the four Si NPs are shown in the **Figure 2**. The PLE spectra of all four samples show similar profiles as their absorption spectra (Figure 1); both show three transitions with matching energies. The two intense and narrow bands at ~ 360 nm and ~ 260 nm are pronounced in the PLE excitation spectra, which indicates that electrons excited through these two transitions can decay to the lower excited-state level and then decay radiatively by photoluminescence. In addition, all four of the surface-modified Si NP samples are ~ 2.5–3.5 nm in size, as shown in TEM (Figure 2A).

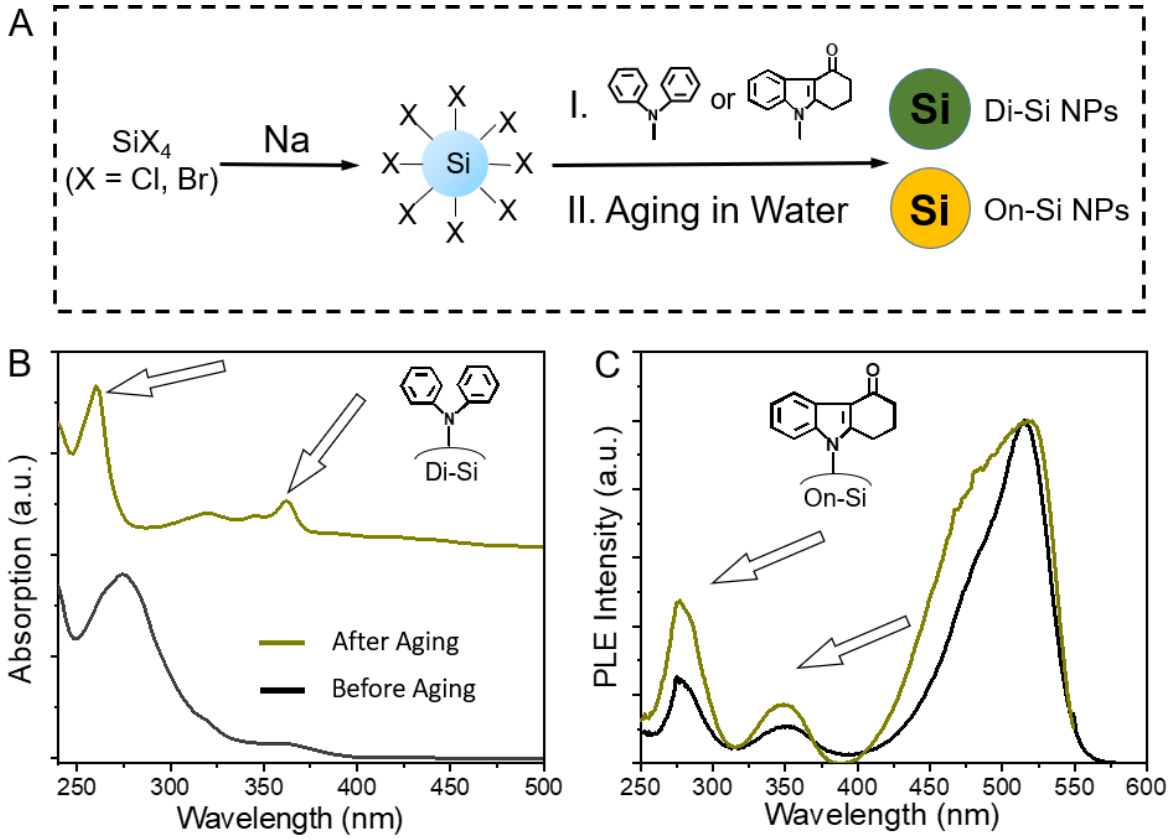

Figure 3. (A) Schematic of the processes of synthesis, surface modification and aging in water. (B) Absorption of Di-Si NPs before and after aging. (C) The PLE spectra of On–Si NPs before and after aging. Arrows indicate the two emerging intense transitions during aging.

To unravel the origin and mechanism of the two anomalous, sharp transitions at ~260 nm and ~360 nm, we monitor absorption and PLE spectra during synthesis and aging (**Figure 3A**). In the Di-Si NPs, we see that the two intense absorption bands at 260 nm and 360 nm gradually

narrow after the NPs were transferred to water (Figure 3B). In addition, it was found that these absorption peaks at 360 nm and 260 nm do not become narrower if oxygen is removed from the water by bubbling with N_2 during the aging process. This result suggests that the oxidation is responsible for the narrowing of the absorption peaks. This oxidation also enhances PL during aging (Figure S2). For On-Si NPs and the other NPs, the two transitions at ~ 360 nm and ~ 260 nm increase in intensity during aging, but do not become significantly more narrow (Figure 3C). In addition, the PL does not change significantly during aging. Previous work on porous silicon and silica-based nanostructures showed PLE spectra with peaks at ~260 nm and ~360 nm.[41–44] Takashi *et al.* proposed that the formation of a defect pair consisting of a dioxasilirane = Si (O_2) and a silylene = Si center has the corresponding electronic transition energies of ~3.5 and ~5 eV.[41] These transitions are similar as the band-I and band-II transitions of our Si NPs. However, unlike the color-tunable PL of our Si NPs, blue emissions were reported in the silicon and silica nanostructures.[41,42,44] The origins of this are typically attributed to oxygen-related defects.

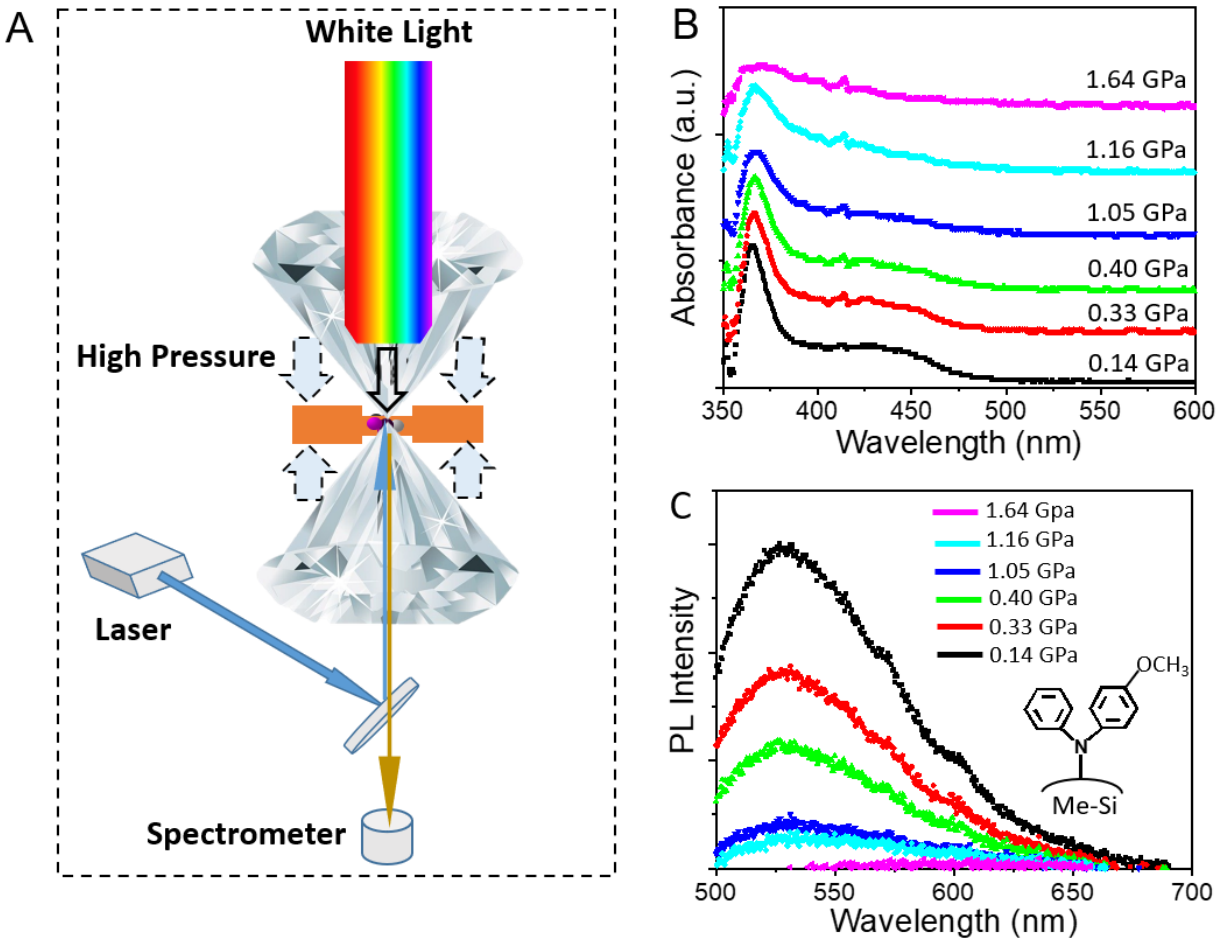

Figure 4. (A) Schematic of the high-pressure optical setup. (B) Pressure-dependent absorption and (C) PL spectra of Me-Si NPs in water (non-hydrostatic pressure medium).

High-pressure optical measurements were conducted on the Me- and On- Si NPs (**Figure 4**) to investigate the nature of the two intense absorption peaks and the strong PL in our Si NPs, and compare this behavior to that of other silicon-based nanostructures. It can be observed that the near-band-edge absorption peak from 400–500 nm (band III) and the PL of Me-Si NPs gradually disappear as pressure is increased to ~1.6 GPa (Figure 4B and 4C**)**. On the other hand, the high-energy absorption peak at 360 nm (band II) remains the same, and does not shift in energy under increasing pressure. These pressure-dependent results indicate that the underlying structural origin of band III and the PL are the same, while the band II at ~360 nm may arise from a different structural origin. Generally, organic compounds with flexible phenyl rings are "soft" and thus are very sensitive to the increasing pressure,[45,46] while inorganic silica is "hard" (bulk modulus ~ 36 GPa) and significant change in the related optical transition is not predicted to occur at this pressure below 1 GPa[47–49]. Thus, this pressure dependence indicates that band II absorption at ~360 nm is related to silicon oxidation, and the PL and band III absorption are related to the ligands.

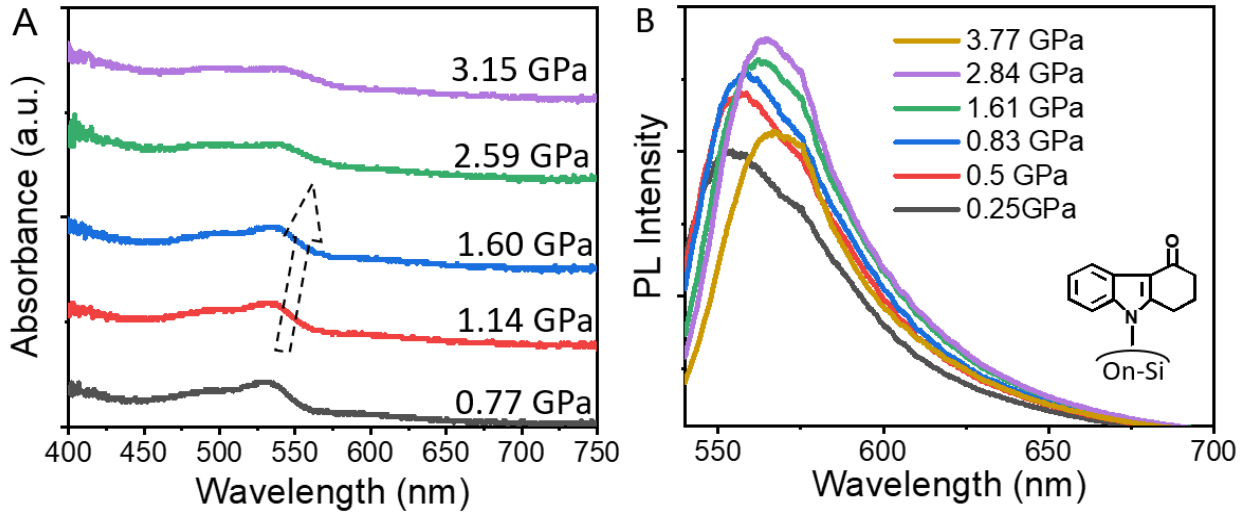

Figure 5. Pressure-dependent (A) absorption and (B) PL spectra of On-Si NPs.

The On-Si NPs with "more rigid" On-ligand in which the two phenyl rings are linked with a C-C bond, was also studied under the high-pressure (**Figure 5A and 5B)**. Similar absorption and PL are observed when water (non-hydrostatic pressure medium) or methanol/ethanol 4:1 (hydrostatic pressure medium) is used as the pressure medium. It was observed that the band III

absorption which was originally at 520 nm red-shifts to 540 nm. The PL also red-shifts from 550 nm to 570 nm. This similar pressure-dependent red-shift again suggests the same structural origin of these two transitions. The red-shift is generally observed in high-pressure studies of organic molecules in which charge transfer is involved in luminescence.[50,51] We plot the PL energy–pressure curve in Figure S3; it can be observed that the PL energy monotonically decreases in response to increasing pressure up to ~ 4 GPa. A linear fitting of the PL emission maximum versus pressure for On-Si NPs yields a value of −9.9 meV/GPa, which is lower than the pressure-dependence values of the quantum-confinement PL from Si nanocrystals,[52] and also lower than the pressure-dependence values (-15 to -20 meV/GPa) for the bandgap of bulk silicon.[53] The PL intensity of On-Si NPs increases with the pressure up to 2.84 GPa, which is in contrast to the Me-Si NPs which showed a significant pressure-induced quenching. Such a pressure-induced PL enhancement is not common in charge-transfer governed luminescent materials, which might arise from the increased proximity of the ligand and surface silicon atoms. Overall, these high-pressure results show that the PL in our Si NPs depends on the structures of the ligands. Such a ligand-dependent result is significantly different from previous high-pressure study on other Si nanoparticles[52] which showed similar pressure-dependence as the bulk silicon. This indicates that the PL arises from the ligand-Si band in our surface-modified Si NPs.

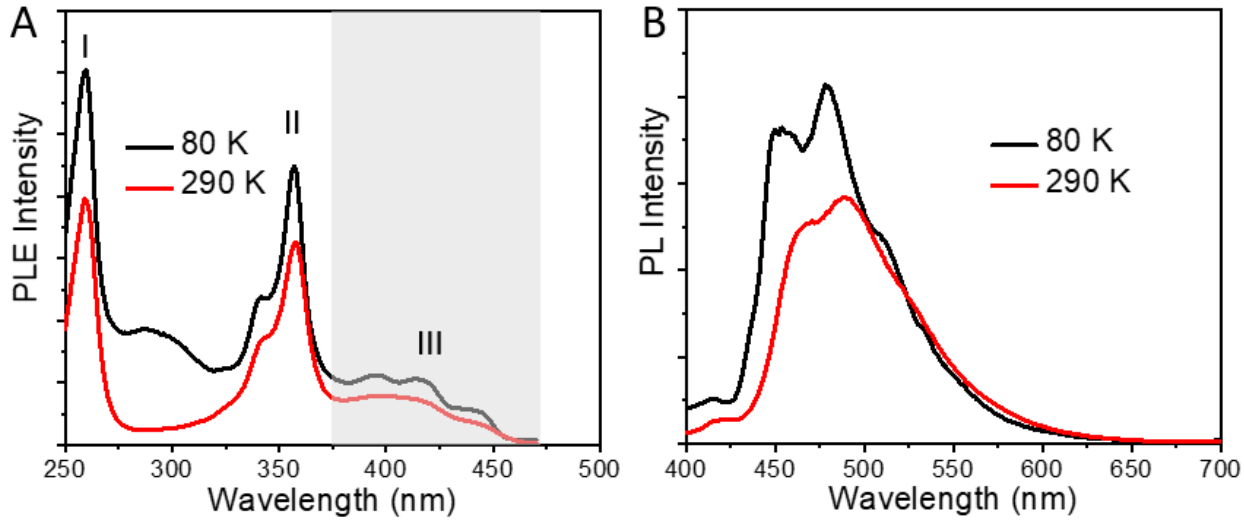

Figure 6. Temperature-dependent (A) PLE and (B) PL spectra of the Ca- Si NPs.

Low-temperature measurements also support these results. As shown in **Figure 6A**, the lowest-energy band-III absorption splits into three peaks when temperature is reduced from room

temperature to 80 K. This is also observed in the PL spectra (**Figure 5B**). The similar splitting of the PLE III and PL, together with the obvious overlap in energies, are further proof that these two transitions are arise from the same structural origin. This is consistent with the pressure-dependent results. Generally, emissive structures containing organic groups show the splitting of PL peaks upon the decrease of temperature. On the other hand, no splitting can be observed for both the PLE peak I and PLE peak II. This indicates that band-I and band-II are related, and have a different structural origin than the band-III and PL.

Scheme I provides a summary of the optical excitations and emissions in our surface-modified/oxidized Si NPs based on the experimental results. Two kinds of optical transitions, the surface oxide bands (I and II) and the ligand-to-Si charge transfer band (III), are identified. We conclude that the electrons that are excited through both surface oxide bands are quickly trapped by the Si-ligand sites, which gives rise to the ultra-bright emission through the ligand-to-Si charge transfer band. The energy of the Si-ligand band is controlled by the structures of the ligands.

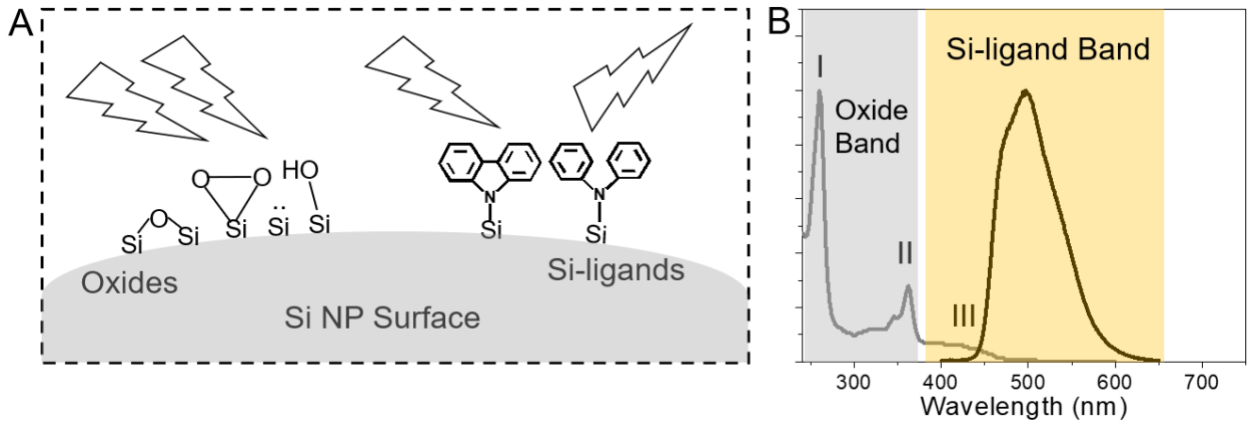

Scheme 1. Optical transitions in surface-modified and oxidized Si NPs. (A) Schematic diagram of the excitation and emission at surface oxides and ligand-Si charge transfer sites. (B) Optical spectra correlated with the oxide bands and the ligand-Si band.

Conclusion. In conclusion, this work reveals that surface oxidation leads to intense transitions in Si NPs. Photoluminescence in these NPs occurs when electrons are excited from the oxide bands and then recombine through the ligand-to-Si charge transfer band. The pressure-dependence of PL in these series of Si NPs is largely dependent on the structures of ligands. Either pressure-induced enhancement and quenching is observed in different Si NPs. Overall, all insights constitute a comprehensive understanding of the optical transitions in surface modified/oxidized

Si NPs with ultrabright PL. The oxidation- and pressure-induced enhancement of optical transitions observed in these Si NPs may be used to design other luminescent nanomaterials in the future.

Methods and Materials. Details are shown in the supporting information.

Acknowledgements. Q.L. and X.W.G. acknowledge funding from the National Science Foundation (DMR-2002936/2002891). Part of this work was performed at the Stanford Nano Shared Facilities (SNSF), which is supported by the National Science Foundation under award ECCS-1542152. R.J. acknowledges financial support from the National Science Foundation (DMR-1808675).

References

(1) Canham, L. T. Silicon Quantum Wire Array Fabrication by Electrochemical and Chemical Dissolution of Wafers. *Appl. Phys. Lett.* **1998**, *APLCLASS2019* (1), 1046–1048.

(2) Calcott, P. D. J.; Nash, K. J.; Canham, L. T.; Kane, M. J.; Brumhead, D. Spectroscopic Identification of the Luminescence Mechanism of Highly Porous Silicon. *Journal of Luminescence* **1993**, *57* (1), 257–269.

(3) Cullis, A. G.; Canham, L. T. Visible Light Emission Due to Quantum Size Effects in Highly Porous Crystalline Silicon. *Nature* **1991**, *353* (6342), 335–338.

(4) Cheng, X.; B. Lowe, S.; J. Reece, P.; Justin Gooding, J. Colloidal Silicon Quantum Dots: From Preparation to the Modification of Self-Assembled Monolayers (SAMs) for Bio-Applications. *Chemical Society Reviews* **2014**, *43* (8), 2680–2700.

(5) Peng, F.; Su, Y.; Zhong, Y.; Fan, C.; Lee, S.-T.; He, Y. Silicon Nanomaterials Platform for Bioimaging, Biosensing, and Cancer Therapy. *Acc. Chem. Res.* **2014**, *47* (2), 612–623.

(6) McVey, B. F. P.; Tilley, R. D. Solution Synthesis, Optical Properties, and Bioimaging Applications of Silicon Nanocrystals. *Acc. Chem. Res.* **2014**, *47* (10), 3045–3051.

(7) Dasog, M.; Kehrle, J.; Rieger, B.; Veinot, J. G. C. Silicon Nanocrystals and Silicon-Polymer Hybrids: Synthesis, Surface Engineering, and Applications. *Angewandte Chemie International Edition* **2016**, *55* (7), 2322–2339.

(8) Priolo, F.; Gregorkiewicz, T.; Galli, M.; Krauss, T. F. Silicon Nanostructures for Photonics and Photovoltaics. *Nature Nanotechnology* **2014**, *9* (1), 19–32.

(9) He, Y.; Fan, C.; Lee, S.-T. Silicon Nanostructures for Bioapplications. *Nano Today* **2010**, *5* (4), 282–295.

(10) Dohnalová, K.; Gregorkiewicz, T.; Kůsová, K. Silicon Quantum Dots: Surface Matters. *J. Phys.: Condens. Matter* **2014**, *26* (17), 173201.

(11) Ding, Z.; Quinn, B. M.; Haram, S. K.; Pell, L. E.; Korgel, B. A.; Bard, A. J. Electrochemistry and Electrogenerated Chemiluminescence from Silicon Nanocrystal Quantum Dots. *Science* **2002**, *296* (5571), 1293–1297.

(12) Meinardi, F.; Ehrenberg, S.; Dhamo, L.; Carulli, F.; Mauri, M.; Bruni, F.; Simonutti, R.; Kortshagen, U.; Brovelli, S. Highly Efficient Luminescent Solar Concentrators Based on Earth-Abundant Indirect-Bandgap Silicon Quantum Dots. *Nature Photonics* **2017**, *11* (3), 177–185.

(13) Gu, L.; Hall, D. J.; Qin, Z.; Anglin, E.; Joo, J.; Mooney, D. J.; Howell, S. B.; Sailor, M. J. In Vivo Time-Gated Fluorescence Imaging with Biodegradable Luminescent Porous Silicon Nanoparticles. *Nature Communications* **2013**, *4* (1), 1–7.

(14) Park, J.-H.; Gu, L.; von Maltzahn, G.; Ruoslahti, E.; Bhatia, S. N.; Sailor, M. J. Biodegradable Luminescent Porous Silicon Nanoparticles for in Vivo Applications. *Nature Materials* **2009**, *8* (4), 331–336.

(15) Zhong, Y.; Peng, F.; Wei, X.; Zhou, Y.; Wang, J.; Jiang, X.; Su, Y.; Su, S.; Lee, S.-T.; He, Y. Microwave-Assisted Synthesis of Biofunctional and Fluorescent Silicon Nanoparticles Using Proteins as Hydrophilic Ligands. *Angewandte Chemie International Edition* **2012**, *51* (34), 8485–8489.

(16) Li, Q.; Niu, W.; Liu, X.; Chen, Y.; Wu, X.; Wen, X.; Wang, Z.; Zhang, H.; Quan, Z. Pressure-Induced Phase Engineering of Gold Nanostructures. *J. Am. Chem. Soc.* **2018**, *140* (46), 15783–15790.

(17) Anthony, R. J.; Cheng, K.-Y.; Holman, Z. C.; Holmes, R. J.; Kortshagen, U. R. An All-Gas-Phase Approach for the Fabrication of Silicon Nanocrystal Light-Emitting Devices. *Nano Lett.* **2012**, *12* (6), 2822–2825.

(18) Lin, T.; Liu, X.; Zhou, B.; Zhan, Z.; Cartwright, A. N.; Swihart, M. T. A Solution-Processed UV-Sensitive Photodiode Produced Using a New Silicon Nanocrystal Ink. *Advanced Functional Materials* **2014**, *24* (38), 6016–6022.

(19) Mangolini, L.; Thimsen, E.; Kortshagen, U. High-Yield Plasma Synthesis of Luminescent Silicon Nanocrystals. *Nano Lett.* **2005**, *5* (4), 655–659.

(20) Pi, X. D.; Liptak, R. W.; Nowak, J. D.; Wells, N. P.; Carter, C. B.; Campbell, S. A.; Kortshagen, U. Air-Stable Full-Visible-Spectrum Emission from Silicon Nanocrystals Synthesized by an All-Gas-Phase Plasma Approach. *Nanotechnology* **2008**, *19* (24), 245603.

(21) Hessel, C. M.; Henderson, E. J.; Veinot, J. G. C. Hydrogen Silsesquioxane: A Molecular Precursor for Nanocrystalline Si−SiO2 Composites and Freestanding Hydride-Surface-Terminated Silicon Nanoparticles. *Chem. Mater.* **2006**, *18* (26), 6139–6146.

(22) Hessel, C. M.; Reid, D.; Panthani, M. G.; Rasch, M. R.; Goodfellow, B. W.; Wei, J.; Fujii, H.; Akhavan, V.; Korgel, B. A. Synthesis of Ligand-Stabilized Silicon Nanocrystals with Size-Dependent Photoluminescence Spanning Visible to Near-Infrared Wavelengths. *Chem. Mater.* **2012**, *24* (2), 393–401.

(23) Shirahata, N.; Nakamura, J.; Inoue, J.; Ghosh, B.; Nemoto, K.; Nemoto, Y.; Takeguchi, M.; Masuda, Y.; Tanaka, M.; Ozin, G. A. Emerging Atomic Energy Levels in Zero-Dimensional Silicon Quantum Dots. *Nano Lett.* **2020**.

(24) Chandra, S.; Masuda, Y.; Shirahata, N.; Winnik, F. M. Transition-Metal-Doped NIR-Emitting Silicon Nanocrystals. *Angewandte Chemie International Edition* **2017**, *56* (22), 6157–6160.

(25) Zhong, Y.; Peng, F.; Bao, F.; Wang, S.; Ji, X.; Yang, L.; Su, Y.; Lee, S.-T.; He, Y. Large-Scale Aqueous Synthesis of Fluorescent and Biocompatible Silicon Nanoparticles and Their Use as Highly Photostable Biological Probes. *J. Am. Chem. Soc.* **2013**, *135* (22), 8350–8356.

(26) Zhong, Y.; Song, B.; Shen, X.; Guo, D.; He, Y. Fluorescein Sodium Ligand-Modified Silicon Nanoparticles Produce Ultrahigh Fluorescence with Robust PH- and Photo-Stability. *Chemical Communications* **2019**, *55* (3), 365–368.

(27) K. Baldwin, R.; A. Pettigrew, K.; Ratai, E.; P. Augustine, M.; M. Kauzlarich, S. Solution Reduction Synthesis of Surface Stabilized Silicon Nanoparticles. *Chemical Communications* **2002**, *0* (17), 1822–1823.

(28) Zhong, Y.; Sun, X.; Wang, S.; Peng, F.; Bao, F.; Su, Y.; Li, Y.; Lee, S.-T.; He, Y. Facile, Large-Quantity Synthesis of Stable, Tunable-Color Silicon Nanoparticles and Their Application for Long-Term Cellular Imaging. *ACS Nano* **2015**, *9* (6), 5958–5967.

(29) Dasog, M.; Yang, Z.; Regli, S.; Atkins, T. M.; Faramus, A.; Singh, M. P.; Muthuswamy, E.; Kauzlarich, S. M.; Tilley, R. D.; Veinot, J. G. C. Chemical Insight into the Origin of Red and Blue Photoluminescence Arising from Freestanding Silicon Nanocrystals. *ACS Nano* **2013**, *7* (3), 2676–2685.

(30) Dasog, M.; De los Reyes, G. B.; Titova, L. V.; Hegmann, F. A.; Veinot, J. G. C. Size vs Surface: Tuning the Photoluminescence of Freestanding Silicon Nanocrystals Across the Visible Spectrum via Surface Groups. *ACS Nano* **2014**, *8* (9), 9636–9648.

(31) Sinelnikov, R.; Dasog, M.; Beamish, J.; Meldrum, A.; Veinot, J. G. C. Revisiting an Ongoing Debate: What Role Do Surface Groups Play in Silicon Nanocrystal Photoluminescence? *ACS Photonics* **2017**, *4* (8), 1920–1929.

(32) Wolkin, M. V.; Jorne, J.; Fauchet, P. M.; Allan, G.; Delerue, C. Electronic States and Luminescence in Porous Silicon Quantum Dots: The Role of Oxygen. *Phys. Rev. Lett.* **1999**, *82* (1), 197–200.

(33) Kůsová, K.; Cibulka, O.; Dohnalová, K.; Pelant, I.; Valenta, J.; Fučíková, A.; Žídek, K.; Lang, J.; Englich, J.; Matějka, P.; Štěpánek, P.; Bakardjieva, S. Brightly Luminescent Organically Capped Silicon Nanocrystals Fabricated at Room Temperature and Atmospheric Pressure. *ACS Nano* **2010**, *4* (8), 4495–4504.

(34) Hannah, D. C.; Yang, J.; Kramer, N. J.; Schatz, G. C.; Kortshagen, U. R.; Schaller, R. D. Ultrafast Photoluminescence in Quantum-Confined Silicon Nanocrystals Arises from an Amorphous Surface Layer. *ACS Photonics* **2014**, *1* (10), 960–967.

(35) Li, Q.; He, Y.; Chang, J.; Wang, L.; Chen, H.; Tan, Y.-W.; Wang, H.; Shao, Z. Surface-Modified Silicon Nanoparticles with Ultrabright Photoluminescence and Single-Exponential Decay for Nanoscale Fluorescence Lifetime Imaging of Temperature. *J. Am. Chem. Soc.* **2013**, *135* (40), 14924–14927.

(36) Li, Q.; Luo, T.-Y.; Zhou, M.; Abroshan, H.; Huang, J.; Kim, H. J.; Rosi, N. L.; Shao, Z.; Jin, R. Silicon Nanoparticles with Surface Nitrogen: 90% Quantum Yield with Narrow Luminescence Bandwidth and the Ligand Structure Based Energy Law. *ACS Nano* **2016**, *10* (9), 8385–8393.

(37) Wang, L.; Li, Q.; Wang, H.-Y.; Huang, J.-C.; Zhang, R.; Chen, Q.-D.; Xu, H.-L.; Han, W.; Shao, Z.-Z.; Sun, H.-B. Ultrafast Optical Spectroscopy of Surface-Modified Silicon Quantum Dots: Unraveling the Underlying Mechanism of the Ultrabright and Color-Tunable Photoluminescence. *Light: Science & Applications* **2015**, *4* (1), e245–e245.

(38) Huang, J.; Li, Q.; Shao, Z. Fabricating Highly Luminescent Solid Hybrids Based on Silicon Nanoparticles: A Simple, Versatile and Green Method. *Nanoscale* **2018**, *10* (21), 10250–10255.

(39) So, W. Y.; Li, Q.; Legaspi, C. M.; Redler, B.; Koe, K. M.; Jin, R.; Peteanu, L. A. Mechanism of Ligand-Controlled Emission in Silicon Nanoparticles. *ACS Nano* **2018**, *12* (7), 7232–7238.

(40) Mastronardi, M. L.; Henderson, E. J.; Puzzo, D. P.; Ozin, G. A. Small Silicon, Big Opportunities: The Development and Future of Colloidally-Stable Monodisperse Silicon Nanocrystals. *Advanced Materials* **2012**, *24* (43), 5890–5898.

(41) Uchino, T.; Kurumoto, N.; Sagawa, N. Structure and Formation Mechanism of Blue-Light-Emitting Centers in Silicon and Silica-Based Nanostructured Materials. *Phys. Rev. B* **2006**, *73* (23), 233203.

(42) Vaccaro, L.; Morana, A.; Radzig, V.; Cannas, M. Bright Visible Luminescence in Silica Nanoparticles. *J. Phys. Chem. C* **2011**, *115* (40), 19476–19481.

(43) Anjiki, A.; Uchino, T. Visible Photoluminescence from Photoinduced Molecular Species in Nanometer-Sized Oxides: Crystalline Al2O3 and Amorphous SiO2 Nanoparticles. *J. Phys. Chem. C* **2012**, *116* (29), 15747–15755.

(44) Qin, G. G.; Liu, X. S.; Ma, S. Y.; Lin, J.; Yao, G. Q.; Lin, X. Y.; Lin, K. X. Photoluminescence Mechanism for Blue-Light-Emitting Porous Silicon. *Phys. Rev. B* **1997**, *55* (19), 12876–12879.

(45) Yuan, H.; Wang, K.; Yang, K.; Liu, B.; Zou, B. Luminescence Properties of Compressed Tetraphenylethene: The Role of Intermolecular Interactions. *J. Phys. Chem. Lett.* **2014**, *5* (17), 2968–2973.
(46) Nagura, K.; Saito, S.; Yusa, H.; Yamawaki, H.; Fujihisa, H.; Sato, H.; Shimoikeda, Y.; Yamaguchi, S. Distinct Responses to Mechanical Grinding and Hydrostatic Pressure in Luminescent Chromism of Tetrathiazolylthiophene. *J. Am. Chem. Soc.* **2013**, *135* (28), 10322–10325.
(47) Bykova, E.; Bykov, M.; Černok, A.; Tidholm, J.; Simak, S. I.; Hellman, O.; Belov, M. P.; Abrikosov, I. A.; Liermann, H.-P.; Hanfland, M.; Prakapenka, V. B.; Prescher, C.; Dubrovinskaia, N.; Dubrovinsky, L. Metastable Silica High Pressure Polymorphs as Structural Proxies of Deep Earth Silicate Melts. *Nature Communications* **2018**, *9* (1), 1–8.
(48) Prescher, C.; Prakapenka, V. B.; Stefanski, J.; Jahn, S.; Skinner, L. B.; Wang, Y. Beyond Sixfold Coordinated Si in SiO2 Glass at Ultrahigh Pressures. *PNAS* **2017**.
(49) Zhou, W.; Shen, H.; Harvey, J. F.; Lux, R. A.; Dutta, M.; Lu, F.; Perry, C. H.; Tsu, R.; Kalkhoran, N. M.; Namavar, F. High Pressure Optical Investigation of Porous Silicon. *Appl. Phys. Lett.* **1992**, *61* (12), 1435–1437.
(50) Lang, J. M.; Dreger, Z. A.; Drickamer, H. G. High-Pressure Luminescence Studies on the Twisted Intramolecular Charge Transfer Molecule 4-(N,N-Dimethylamino)Benzonitrile in Polymer Matrixes. *J. Phys. Chem.* **1994**, *98* (44), 11308–11315.
(51) Dai, Y.; Zhang, S.; Liu, H.; Wang, K.; Li, F.; Han, B.; Yang, B.; Zou, B. Pressure Tuning Dual Fluorescence of 4-(N,N-Dimethylamino)Benzonitrile. *J. Phys. Chem. C* **2017**, *121* (9), 4909–4916.
(52) Hannah, D. C.; Yang, J.; Podsiadlo, P.; Chan, M. K. Y.; Demortière, A.; Gosztola, D. J.; Prakapenka, V. B.; Schatz, G. C.; Kortshagen, U.; Schaller, R. D. On the Origin of Photoluminescence in Silicon Nanocrystals: Pressure-Dependent Structural and Optical Studies. *Nano Lett.* **2012**, *12* (8), 4200–4205.
(53) Slykhouse, T. E.; Drickamer, H. G. The Effect of Pressure on the Optical Absorption Edge of Germanium and Silicon. *Journal of Physics and Chemistry of Solids* **1958**, *7* (2), 210–213.